Multi-scale experimental analysis of rate dependent metal-elastomer interface mechanics

J. Neggers[a], J.P.M. Hoefnagels[a,*], O. van der Sluis[b,a], M.G.D. Geers[a]

[a]*Eindhoven University of Technology, Department of Mechanical Engineering, Den Dolech 2, 5612 AZ Eindhoven, The Netherlands*
[b]*Philips Research, High Tech Campus 34, 5656 AE Eindhoven, Netherlands*

Abstract

A remarkable high fracture toughness is sometimes observed for interfaces between materials with a large elastic mismatch, which is reported to be caused by the fibrillar microstructure appearing in the fracture process zone. In this work, this fibrillation mechanism is investigated further to investigate how this mechanism is dissipating energy. For that purpose, thermoplastic urethane(TPU)-copper interfaces are delaminated at various rates in a peel test experimental setup. The fracture process zone is visualized *in situ* at the meso scale using optical microscopy and at the micro scale using Environmental Scanning Electron Microscopy (ESEM). It is shown that the geometry of the fracture process zone is insensitive to the delamination rate, while the interface traction scales logarithmically with the rate. This research has revealed that, the interface roughness is shown to be pivotal in initiating the fibrillation delamination process, which facilitates the high fracture toughness. The multi-scale experimental approach identified two mechanism responsible for this high fracture toughness. Namely, the viscous dissipation of the TPU at the high strain levels occurring in the fibrils and the loss of stored elastic energy which is disjointed from the propagation due to the size of the process zone.

Keywords: delamination, fracture toughness, multi-scale, rubber material, mechanical testing

1. Introduction

Interfaces between materials with a large elastic mismatch are of increasing scientific and industrial interest, as they are more frequently used in advanced engineering materials and devices, including, e.g., composites [12], coatings [18], microelectronics [27, 20], and flexible [22, 26] and stretchable electronics [16, 8]. The main benefit of the synergy between these materials lies in combining the high stiffness of one material with the high toughness and compliance of the other, usually soft material. Major improvements in material properties can be achieved if the interfaces are strong enough to transfer the applied loads and deformations. Consequently, interface failure often is a precursor to failure [14, 21, 7]. Improving the interface properties thereby generally improves the robustness of multi-layered devices.

Previously, a two elastomer-metal interface system is discussed with a large elastic mismatch and a large interface roughness, for which a remarkably high macroscopic fracture toughness was

*Corresponding author. Phone: +31-40-247-4060; E-mail: j.p.m.hoefnagels@tue.nl

observed ($G_c > 2$ kJ/m^2) [6]. The coarse scale toughness largely exceeds the adhesion energy of metal-rubber valence bonds, reported to be in the range of $0.1 < \Gamma_{ad} < 10$ J/m^2 [2, 3, 1]. *In-situ* observation of the delaminating peel front of these interfaces reveal the formation of microscopic fibrils. However, the exact micromechanical origin of the enhanced fracture toughness is so far poorly understood. To enable the engineering of interfaces with enhanced fracture toughness, it is important to understand the underlying mechanics that amplifies the fracture toughness of these interface systems.

Therefore, the goal of this paper is to unravel the delamination micromechanics which are responsible for dissipating the large quantities of energy in such ductile interfaces. To this end, the 'ThermoPlastic Urethane (TPU)'-copper interface system will serve as a model system for this investigation. The strategy departs from *in-situ* high-magnification visualization of the delaminating TPU-copper peel front for different copper roughnesses. The interface micromechanics are evaluated at a large range of peel rates to investigate delamination rate sensitivity and to possibly activate different dissipation mechanisms without altering the interfaces.

2. Experimental methodology

The samples are created from commercially available laminated bi-layer TPU-copper foils (TPU: 50 µm Walopur, Epurex; copper: 37 µm TW-YE, ArcelorMittal), similar to what is used in stretchable electronic applications [16, 6]. The TW-YE is a circuit grade, rolled copper foil with one relatively smooth untreated side ($R_a \approx 0.5$ µm) and one rough side, which received an extra electroplating step ($R_a \approx 1.9$ µm). Four-layer specimens are made by laminating two as-received TPU-copper bi-layer foils, enabling peel tests to be performed by clamping and pulling on a copper foil at each specimen arm, effectively creating a T-peel test. Such a T-peel test is chosen because of its optical accessibility and the stationary location of the peel front which is beneficial for imaging at high magnifications.

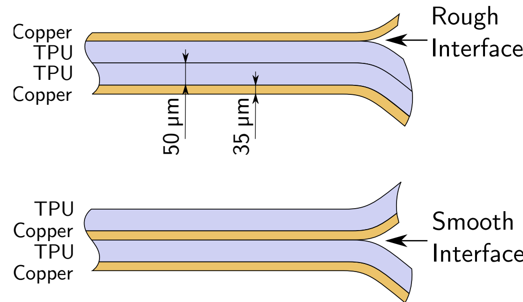

Figure 1: Two sample configurations, where the rough interface type is created by laminating to TPU-copper sheets TPU side to TPU side and the smooth interface type is created by laminating two sheets TPU side to copper side, effectively creating four layer samples.

Sample type 'rough' is created by laminating TPU to TPU at 180 °C, with one part of the foil not laminated to form a pre-crack (figure 1, top figure). Sample type 'smooth' is created by laminating TPU to the smooth copper side (figure 1, bottom figure), using the same lamination procedure to induce as little variation with the rough sample type as possible. Figure 2a shows a cross-section image taken with an optical microscope (Zeiss Discovery V20), which shows that the layer thicknesses are close to the specified thickness. Additionally, a cross-section of

the copper was prepared by polishing a specimen which was embedded in epoxy, for optimal image quality. This cross-section is then imaged in a scanning electron microscope to show the complex roughness topology (figure 2b).

The topography of the smooth and rough side of TW-YE copper foil are measured directly using Confocal Optical Profilometry (Sensofar Plμ2300), see figure 3, clearly showing the contrast in roughness between the two surfaces. Nicely shown is the cauliflower-type topography of the rough surface, which is typical for electroplated metal.

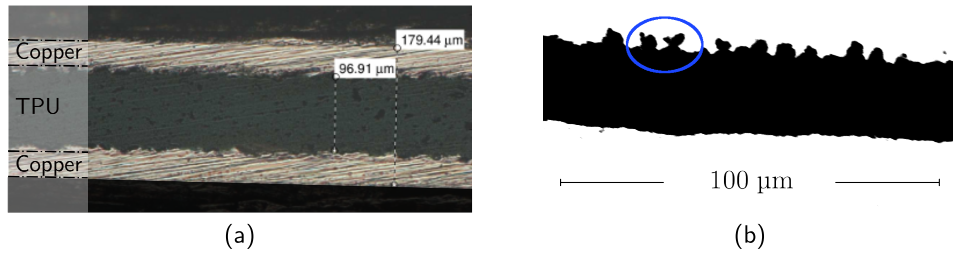

Figure 2: (a) Optical microscope image of the cross-section of the rough interfaces, showing the sample layer thicknesses. (b) An SEM image of copper foil (black) embedded in epoxy (white) to carefully create a polished cross-section, showing the interlocking structures of the rough interface.

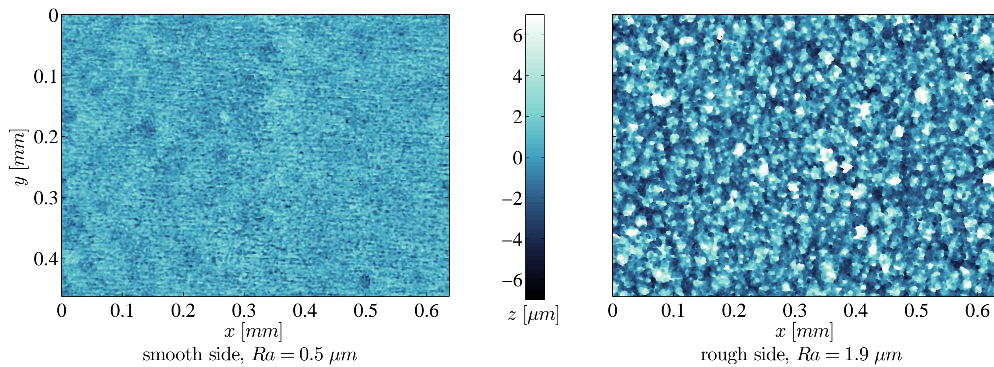

Figure 3: Surface topographies of the two sides of the TW-YE circuit grade rolled copper foil, as measured with confocal profilometry.

The samples are delaminated in a T-peel test or 180° peel test configuration (figure 4a) using the micro-tensile stage (Kammrath & Weiss GmbH) shown in figure 4b. In such a configuration, the two arms of the pre-crack are clamped, while the laminated part of the sample is supported in a low-friction guide to enforce a perpendicular angle with respect to the loading direction, without significantly dissipating energy.

Figure 4: (a) *In-situ* optical microscopy side-view of a T-peel test, showing the large deformations in the TPU near the peel front. (b) The micro-tensile stage mounted in the vacuum chamber of an ESEM.

The tensile stage is small enough to fit underneath the objective of the optical microscope, or inside the vacuum chamber of an environmental scanning electron microscope (ESEM). By using the environmental mode of the ESEM, it is possible to prevent 'charging' effects, enabling high resolution imaging of the TPU. The tensile setup is such that the peel front propagates stationary allowing *in-situ* high magnification ESEM imaging of the progressing delamination front, see e.g. figure 5. This image shows the complex micromechanics at the peel front, which is the focus of investigation in this paper. Note, that the electron beam irradiation might easily alter the fibrillation process. This becomes clear by temporarily exposing the progressing delamination front with a typically-used electron beam intensity, indicated by the rectangles in figure 5. Obviously, influence of the imaging technique on the delamination micromechanics is undesirable. Therefore, a preliminary study was carried out by careful comparison of exposed and unexposed adjacent surfaces, yielding optimized ESEM electron beam settings that stay away from influencing the fibrillation process. As the specific electron beam settings depend on the peel rate, the scanning dwell-time, and the magnification, the imaging settings have separately been optimized for each experiment.

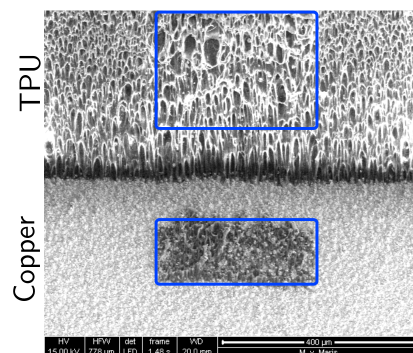

Figure 5: *In-situ* ESEM visualization of the delaminating peel front. In this example the possible influence of the beam on the delamination process is visualized by temporarily exposing the progressing peel front to a higher intensity (blue boxes). For all other ESEM images, the e-beam intensity is optimized to prevent this effect.

3. Results and discussion

3.1. Roughness-induced fibrillation

First, the bulk material behavior of the employed copper foil and TPU sheet are measured, see figure 6, which will serve as a reference for the microscopic analysis. As expected, a large elastic mismatch is visible from the large difference in modulus and fracture strain (copper Young's modulus: $E \approx 86$ GPa, TPU Neo-Hookean modulus: $C_{10} \approx 4$ MPa). Moreover, by comparing the stress-strain data at different strain rates, it becomes clear that the TPU is not a typical hyper-elastic rubber. The material shows an increase in stress level of ~8% for a two times larger strain rate. Additionally the materials shows load-unload hysteresis and permanent deformation after unloading to zero stress. The constant slope between the initial loading and the initial unloading points is usually observed in glassy polymers, indicating that the TPU polymer chain segments show some stress induced mobility, at least at room temperature.

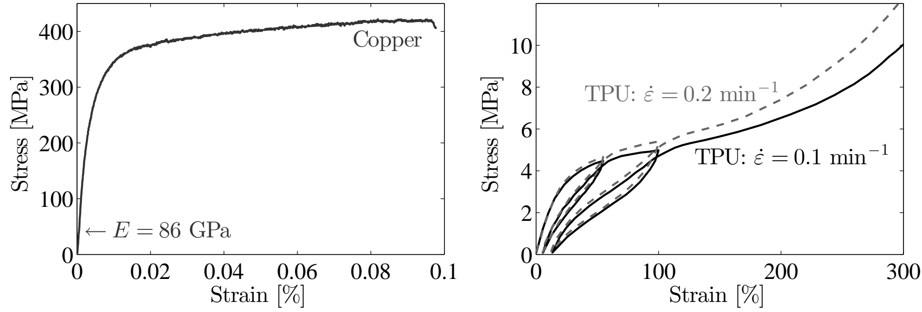

Figure 6: Engineering stress-strain curves, measured from macroscopic uniaxial tensile tests of TW-YE circuit grade rolled copper foil and Walopur TPU sheet (at two strain rates).

Typical force-displacement curves of peel tests of smooth and rough TPU-copper samples are shown in figure 7. The force-displacement curves show the expected trend; a gradual increase of the force during the crack initiation phase, followed by a constant force plateau during the stable crack growth regime. The fracture toughness is characterized by the so-called 'work of separation', WOS, which is defined as the work required to progress the peel front dU, per unit of advanced crack area. Similar to what is commonly done, the WOS is calculated by dividing the applied clamp force F by the specimen width b [11, 13],

$$WOS = \frac{1}{b}\frac{dU}{da} = \frac{F}{b}, \quad (1)$$

where da is the increase in crack length, which in this case is assumed to be equal to the clamp displacement du. The considered experiment both clamps are moving. The direct relation between da and du is assumed reasonable considering that the low peel force does not significantly strain the TPU-copper arms, by which the interface is loaded. The WOS is the macroscopic fracture toughness G_c, and includes many dissipative mechanisms for the meso and micro scales. It is exactly the purpose of this paper to investigate the lower scales and identify these various contributions.

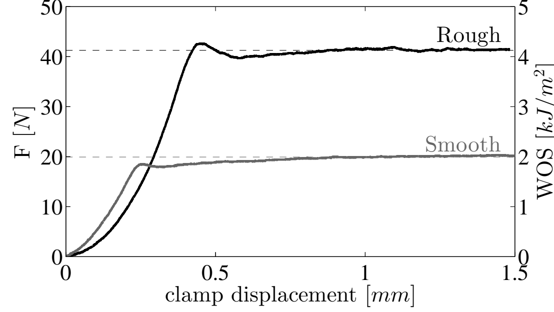

Figure 7: Work of separation (WOS) versus opening displacement for peel tests of the smooth and rough TPU-copper interface samples.

Macroscopically, two main observation can be made: (*i*) the fracture toughness is high, well above 1 kJ/m^2; (*ii*) a significantly larger fracture toughness is found for the rough interface. The latter was expected, as it is well-known from engineered examples that roughness influences the fracture toughness. For instance, the TW-YE copper foil is often used in large-area stretchable electronic products [24, 16, 9] due to its improved adhesion properties. The fracture toughness for the smooth interface was already outstanding, and the increase in fracture toughness caused by the increase in copper surface roughness is even more remarkable.

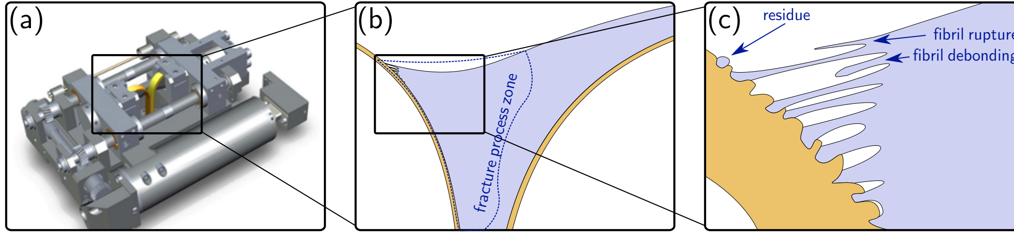

Figure 8: The three length scales at which the delamination process is analyzed, (a) macroscale, (b) mesoscale, (c) microscale.

At the mesoscale, defined here as the scale where typically FEM interface elements are applied, it is reasonable to decompose the WOS into the contribution of the fracture process zone Γ_{fpz} and the remaining part of the sample, i.e. the structural part of the sample Γ_{str}. The structural part contains contributions from the bulk (figure 8), for instance, the plastically dissipated energy due to the bending of the copper films. In a FEM model this would be the represented by the corresponding bulk elements. The decomposition is akin to what is already discussed by Hutchinson and Suo [10]

$$\mathrm{WOS} = \Gamma_{\mathrm{fpz}} + \Gamma_{\mathrm{str}}. \tag{2}$$

The effect of the structural dissipation on the WOS has been discussed before, for instance by Tvergaard and Hutchinson [17] and Wei and Hutchinson [25]. Models based on the WOS tend to be dependent on the geometry and loading conditions of the sample. Instead, in this paper the attention is focused on the relation between the delamination micromechanics and the energy

dissipated at the mesoscale (i.e. in the fracture process zone). Inversely, the above equation defines the fracture process zone as the volume of material contributing to the interface toughness. The numerical equivalent would a cohesive zone, in which the energy of the fracture process zone is lumped, depending on the dissipative contribution of the nearby bulk elements.

For the discussed T-peel test, the only significant structural dissipation component comes from the bending of the 37 μm thick copper films. The maximum strain, and thereby also the amount of plastic flow, is directly related to the bending radius of the copper. This radius was measured from images like the one showed in figure 4a. It was observed that the bending radius of the copper was approximately 300 μm, and did not significantly change between experiments. By performing simulations with cohesive zone interface elements with a traction opening relation, as described by van den Bosch et al. [18] and Hoefnagels et al. [6], it was observed that the structural dissipation was approximately 30% of the WOS for the rough interface. Since the copper film thickness and the peel test geometry remain constant throughout the paper, observed changes in WOS are attributed to changes in the fracture process zone [12].

The fracture process zone dissipation is subdivided into several components,

$$\Gamma_{\text{fpz}} = \Gamma_{\text{ad}} + \Gamma_{\text{efpz}} + \Gamma_{\text{ifpz}}, \tag{3}$$

with Γ_{ad} is the interface adhesion energy required to break the bonds between the materials, Γ_{efpz} is non-recoverable elastic energy in the fracture process zone, and Γ_{ifpz} is energy dissipated by irreversible deformation in the fracture process zone. The adhesion energy is reported to be in the range of $0.1 < \Gamma_{\text{ad}} < 10$ J/m^2 [2, 3, 1], and is therefore assumed negligible considering the WOS > 2 kJ/m^2. The other two terms will be investigated further.

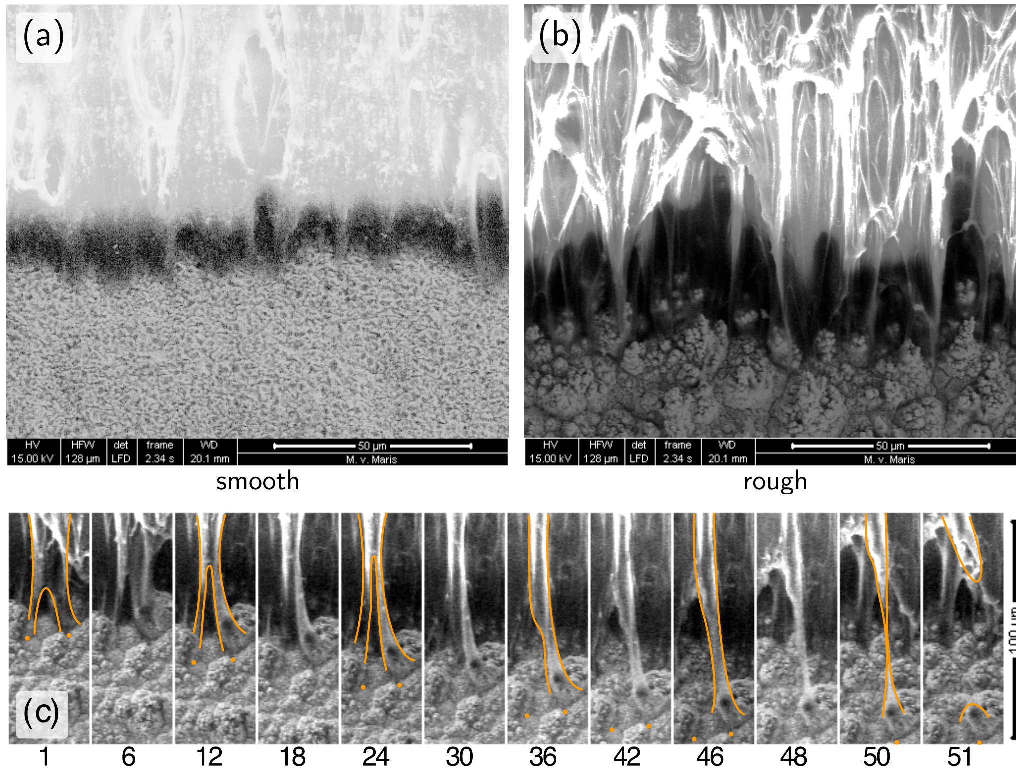

Figure 9: *In-situ* ESEM visualization of a delaminating peel front, showing a distinct difference in micromechanisms of both interface roughnesses. The lower image strip shows the evolution of a fibril up to failure from the rough copper. The numbers denote the image frame numbers, recorded at 1 frame per second. Guidelines have been added to mark the outline of the fibril and the original adhesion point.

Typical examples of *in-situ* ESEM images of the smooth and rough peel front, recorded during steady-state crack growth, are shown in figure 9ab. Both the smooth and rough interface exhibit a fibrillation process, i.e. TPU fibrils are formed. However, pronounced differences are observed. For the rough interface, the fibrils are slender with a large fibril failure length of $L_f \approx 30$ µm, whereas the smooth interface reveals shorter and wider fibrils. The location of the fibrils on the smooth interface does not show a direct relation to the copper topography. Conversely, the rough interface fibrils are connected at the bases of the roughness peaks, implying that their distribution and geometry is initiated by the copper topography. This difference in fibril micromechanics may be related to the fact that only the rough copper surface has sufficiently large and rough protrusions to mechanically interlock the TPU material in the valleys between the protrusions, as can be seen in the detailed view of the cross-section of the rough interface shown in figure 2b.

The evolution of a single fibril up failure is shown in the lower series of images in figure 9. Frame 1 is the first frame where the fibril geometry can be identified. The fibril is attached at a roughness valley and elongates with increasing time. The fibril partially fails in frame 36, after which it continues to be stretched until it finally ruptures leaving TPU residue on the copper surface. From the evolution of this fibril and other studied fibrils some observations are made.

First, extreme elongation of the TPU fibrils occurs, especially for the rough interface. Careful assessment of the evolution of single fibrils shows that the fibrils, after prior significant stretching to become visible at the peel front, typically exhibit a subsequent stretch ratio up to 5 before failure sets in. This corresponds to a TPU fracture strain well beyond the macroscopic TPU strain shown in figure 6b. Ultimately, the fibrils are elongated up to approximately 30 μm until they either rupture or debond from the copper surface.

The rough copper surface creates locally strong interface spots due to mechanical interlocking, which causes large deformations in the soft TPU. Consequently, there is a strong correlation between the distribution of delamination initiation locations and the topology of the copper roughness. Most of the observed fibrils appear to be attached to the roughness valleys, or at least to the sides of the roughness peaks, indicating that the delamination initiates at the roughness peaks. During the final stages the fibril base delaminates from the valley until the fibril is pulled over the roughness peak where it finally fails. Due to the geometry of the roughness, locations with large negative hydrostatic pressure are created at the peaks of the roughness, enhanced by the near incompressibility of the TPU. These hydrostatic stresses are known to initiate voids through cavitation [3, 1] which would thus first occur at the roughness peaks.

The macroscopic peel tests show an increased fracture toughness for the rough sample type, and this extra fracture toughness must be related to the fibrillation process. Since the TPU is not fully hyperelastic, and has shown energy dissipation at the macroscale (figure 6), a part of the energy will be dissipated viscously during the elongation of the fibrils. Nevertheless, it is unlikely that this is the major dissipative mechanism, since the same behavior is observed for PDMS (Polydimethyl Siloxane) which is hyperelastic [6, 19]. Besides irreversible energy, a large portion of elastically stored energy is present in the fracture process zone, Γ_{efpz}. When the fibril fails, the elastically stored energy in the fibril, and in the adjoining TPU material is released. It is hypothesized that the majority of this energy does not contribute the to fracture process but is dynamically lost. In the image strip shown in figure 9, it can be seen that the moment the fibril fails, the distance to the next (younger) fibril is too far to efficiently transfer tractions. Additionally, the complex roughness geometry forces the crack to run along the side of the roughness protrusions, i.e. parallel to the opening direction, which causes crack arrest, or crack branching into the tougher TPU material. Both processes increase the macroscopic fracture toughness.

3.2. Rate dependent peel testing

The rate-dependent response of the TPU at macroscale (figure 6b) triggered an investigation to how this translates to the microscale. To this end, the rough interface is peeled in the T-peel test at various peel rates while measuring the macroscopic fracture toughness and performing *in-situ* analyses of the micromechanisms. The following microscale analyses will consist of a quantification of the fibrillation geometry as a function of peel rate, complemented with a detailed analyses of the post-delamination surfaces.

3.2.1. Peel rate results

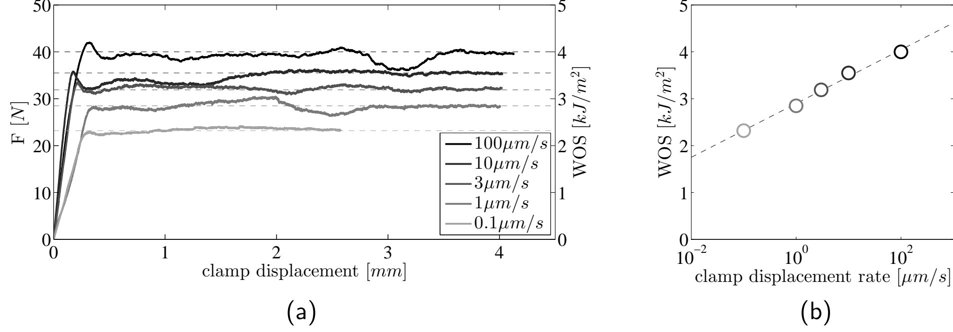

Figure 10: (a) the work of separation (WOS) versus opening displacement for five peel tests, performed at different peel rate, $\dot{u}$, covering three orders of magnitude and (b) the WOS-level at the steady state crack propagation plateau plotted as a function of the logarithm of the peel rate. The logarithmic fit shows a high correlation confidence with a R^2 value of 0.992.

Figure 10 shows the macroscopic experimental data for five typical peel test experiments with peel rates ranging from $\dot{u} = 0.1$ µm/s to $\dot{u} = 100$ µm/s. Interestingly, the measured WOS shows a linear trend with the logarithm of the peel rate,

$$\mathrm{WOS}(\dot{u}) = \alpha \ln \dot{u} + \beta \tag{4}$$

where $\alpha \approx 0.6$ and $\beta \approx 2.9$ are fitted with linear regression ($R^2 = 0.992$).

The mesoscale lift-off geometry is evaluated by imaging the peel test *in-situ* from the side, using optical microscopy. Figure 11 shows three of the analyzed images, illustrating that the deformed geometry is remarkably constant. For instance the radii of the copper foils have been measured by image processing of 20 images per peel rate, and was found to be 300 ± 20 µm, for each peel rate. A constant copper bending radius translates to a constant contribution of the copper plasticity to the WOS. Therefore, changes in measured WOS must be caused by the mechanisms within the fracture process zone.

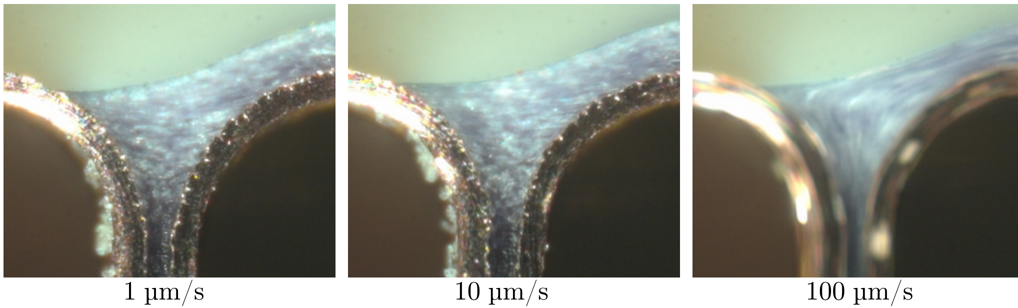

Figure 11: Side-view optical microscopy images of mesoscopic peel front at various peel rates. Note that, although the work of separation in each test is significantly different, the deformed peel test geometry seems independent of the peel rate.

Similarly to the roughness microscale experiments, the progressing peel front is imaged in the ESEM, for various peel rates. Due to frame-rate limitations of the ESEM, the faster peel

rates are not analyzed. Figure 12, shows a typical ESEM image for each peel rate. Analogous to the mesoscale, the fibrillation process shows no significant dependence on the peel rate. This is understandable from the proposed hypothesis, that the fibrillation process is initiated by the interlocking and cavitation mechanisms, which are both determined by the geometry of the copper roughness. Figure 13, shows the measured lengths of the fibrils, just before failure. The uncertainty of the length measurement is estimated at 3 pixels and the impact of an uncertainty in time considering movements during the time between frames. This uncertainty is represented by the gray error bar next to the data points in figure 13. A linear fit through the measured lengths highlights the independence of the fibril failure length on the peel rate.

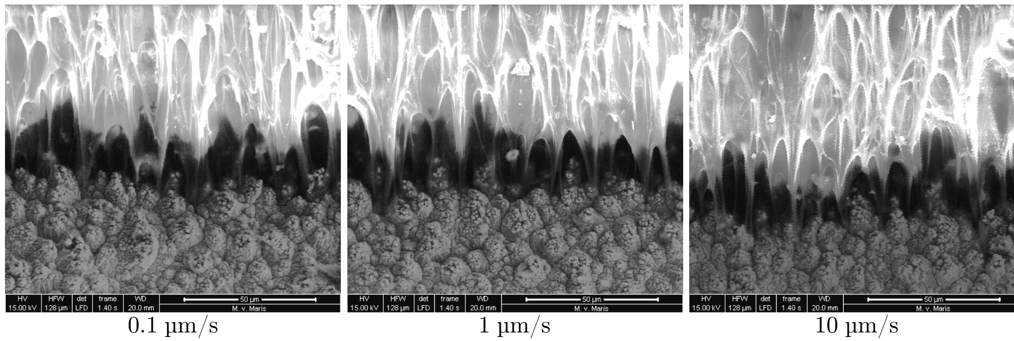

Figure 12: *In-situ* ESEM visualization of the delaminating peel front, showing the fibrillation mechanisms at different peel rates. Interestingly, the fibril geometry appears independent of the peel rate

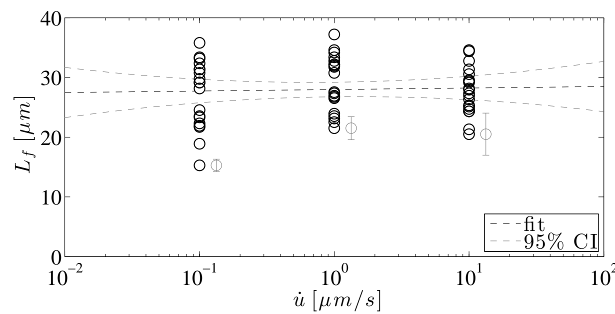

Figure 13: Fibril length measured from *in-situ* microscopic movies of peel tests at various peel rates. The fibril length is measured in the frame before it fractures. The uncertainty for each peel rate is represented by the gray error bar next to the data points.

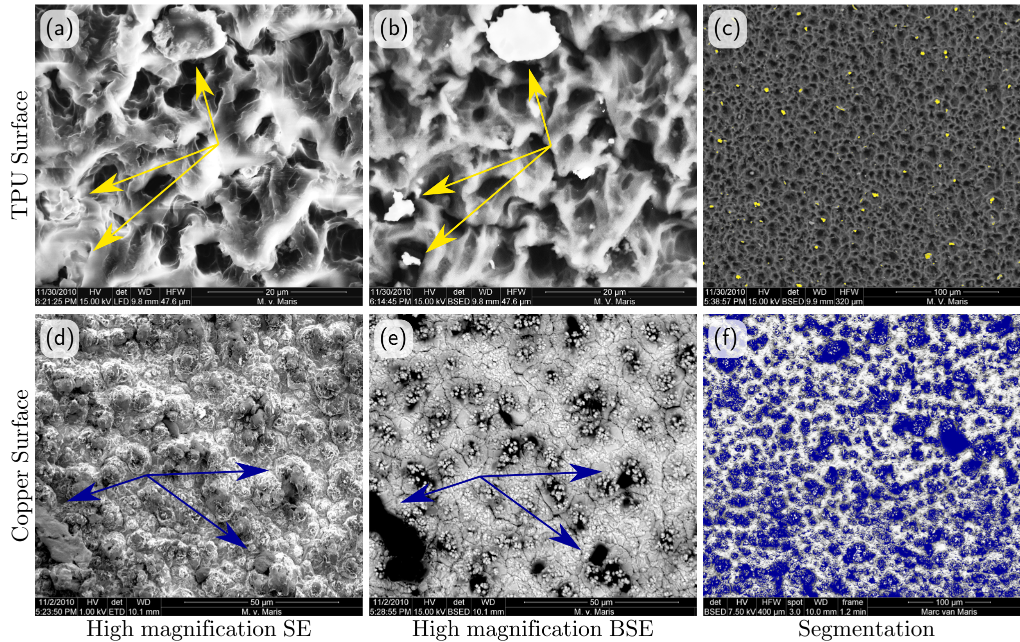

Figure 14: ESEM images of the post delamination TPU surface (a,b,c) and copper surface (d,e,f). On the left the topography of the surface is shown using the secondary electron (SE) detector. The center image is taken at the same location using the back scatter electron (BSE) detector in "z-contrast" mode creating maximum contrast between the copper (bright) and TPU (dark). The right images are typical examples of large-area threshold images, used to segment the image to compute the relative area of residue each surface.

During the detailed fibril evolution investigations it was noticed that some fibrils debond from the interface while others rupture, leaving residue on the copper surface, see figure 8c. Occasionally, a copper roughness peak is pulled off the copper surface, leaving copper residue on the TPU surface. With the z-contrast mode of the back scatter electron detector images are created of both surfaces with high contrast between the heavy atomic mass copper (bright) and the light TPU (dark). A thresholding technique is used to compute the relative area of residue on each surface as a function of the peel rate (figure 14).

In figure 14d and 14e it can be noticed that the TPU residue resides mostly on the roughness peaks. However, the location of TPU residue does not confirm the location where the fibril was adhered. It could be that the fibril end delaminated without leaving residue. The film strip shown in figure 9c shows that, during the final phase the fibril delaminates from the valley and is pulled over the top of the peak. The final point of attachment seems to be the side of the peak, where the copper geometry is interlocking the strongest.

The relative area of residue is measured on a number of high definition images (4096×3536 px) of a large field of view (345×400 µm) for statistical reasons. The measured relative area of copper on the TPU surface A_c for each image is shown in figure 15a, and the relative area of rubber on the copper surface A_r of each image is shown in figure 15b. From these figures a few details are observed: (*i*) The amount of copper residue on the TPU surface is small for all peel rates implying that the copper fracture process does not significantly contribute to the fracture toughness; (*ii*) The amount of copper fracture increases with peel rate. Assuming a

normal probability distribution for the strength of the copper peaks, then more fracture of rough peaks suggests that, on average, the surface experienced higher loads indicating that the tractions in the fibrils increase for increasing peel rates; (*iii*) The significant amount of TPU residue on the copper surface indicates that fibril fracture is an important mechanism; (*iv*) The amount of TPU residue increases for increasing peel rates, demonstrating that more fibrils fracture when the interface is loaded faster.

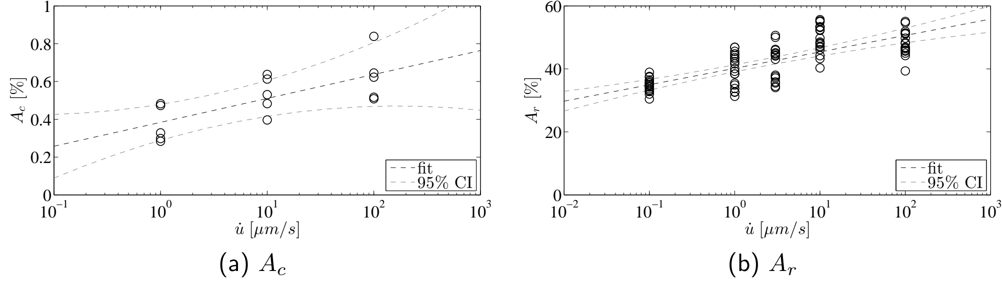

Figure 15: (a) The relative area of copper on the TPU surface, A_c, as a result of the delamination as a function of the peel rate. (b) The relative area of TPU on the copper surface, A_r, as a result of the delamination as a function of the peel rate. Note that both show an increasing trend for increasing peel rates.

3.2.2. Peel rate discussion

Interpretation of the peel rate dependent results starts with the observed increase in fibril traction (i.e. observation (*ii*) above). The TPU showed a viscoelastic response macroscopically (figure 6), from which the higher tractions observed at the micro scale can be explained. Higher tractions in the fibrils may result in the observed higher energy dissipation, either through increased irreversible deformation in the fibrils, or through increased dynamically lost elastic energy. Higher fibril tractions, combined with similar fracture strains, lead to more elastically stored energy which can be dynamically released, in the fibrils and in the bulk material nearby. Similar fracture strains are expected based on the observed peel rate insensitivity on the fibril geometry (microscale) and on the fracture process zone geometry (mesoscale). The amount of dissipation due to irreversible deformation is unknown for these experiments. However, since the volume of material which is reaching the regime where TPU starts behaving glassy is small, the contribution to the fracture toughness will most likely be much smaller than the contribution coming from the dynamic loss of elastic energy, which is in line with the observations made by [23] on PDMS copper interfaces.

Higher tractions in the fibrils imply higher tractions at the copper-fibril interface, from which more fibril debonding would be expected. Interestingly, the TPU residue measurement shows the opposite, i.e. more fibril fracture and less fibril debonding occurs for higher peel rates. This suggests that the adhesion of the fibrils to the copper increases with the peel rate, i.e. the interlocking mechanism is more effective at higher peel rates, which would lead to improved adhesion and therefore more fibril fracture. Delaminating an interlocked area requires that the TPU flows out of the copper geometry. Because the flow stress is naturally rate dependent, this theory is consistent with the observed behavior.

Finally, the fibril fracture length was measured to be independent of the peel rate within measurement uncertainty, suggesting that the fibril fracture strain is also rate independent. Additionally, the mesoscale deformed geometry was also measured to be rate independent within

measurement uncertainty (figure 11), suggesting that the fracture process zone does not change with peel rate. This leads to the assumption that the shape of the traction profile along the fracture process zone is a rate-independent function $f_\tau(\vec{x})$ of the position, and only the traction amplitude $c(\dot{u})$ scales with the peel rate,

$$\tau(\vec{x}, \dot{u}) = c(\dot{u}) f_\tau(\vec{x}), \tag{5}$$

For the T-peel test, the WOS is computed from the measured force, which is balanced by the traction profile of the fracture process zone,

$$\mathrm{WOS}(\dot{u}) b = F(\dot{u}) = \int \tau(\vec{x}, \dot{u})\, \mathrm{d}\vec{x} = c(\dot{u}) \int f_\tau(\vec{x})\, \mathrm{d}\vec{x}. \tag{6}$$

The above equation is essentially a force balance, where a separation in in space and time is made. This separation is only valid if the traction profile is constant over time, and if the amplitude over this profile depends linearly on the logarithm of the peel rate. Moreover, this formulation neglects the rate dependence of any other dissipative mechanisms, such as copper plasticity. The logarithmic relation between the WOS and the peel rate, shown in figure 10b, transfers to the fracture process zone as a logarithmic relation between the flow stress and the strain rate, as also discussed by e.g. Liechti and Wu [15] and Geißler and Kaliske [5]. Such single relaxation time behavior reminds of Eyring flow typically observed in glassy polymers, possibly indicating that stress induced polymer chain mobility is contributing to the rate-dependent fracture toughness observed at the macro scale [4].

4. Conclusions

Interfaces between materials with a large elastic mismatch, which are of increasing interest for advanced engineering materials and applications, may exhibit an exceptionally high fracture toughness. To unravel the micromechanical origin underlying this high toughness, a detailed characterization was conducted on two elastomer-metal (TPU-copper) interfaces, which only differ in the copper surface roughness. To this end, T-peel tests were performed under *in-situ* optical and environmental scanning electron microscopic observation. This enabled a multi-scale experimental analysis that included the macroscopic work of separation, real-time observations of the mesoscopic and microscopic peel front with its underlying micromechanisms, and post-mortem microscopic analyses of the delaminated surfaces. Moreover, the rate dependence of this TPU-copper interface was investigated by comparing the experimental results for peel tests delaminated over three rate decades.

It was found that the interface roughness triggers a fibrillation mechanism at the delamination front, in which micron-sized TPU fibrils are formed with a distribution and geometry that is governed by the copper topography. Specifically for the rough interface, fibrils were clearly shown to be connected at the 'valleys' of the roughness protrusions, and individual fibrils were observed to continue to deform after the peel front passed, thereby exhibiting a huge elongation, until fibril fracture or interface debonding set in. The origin of this fibrillation process, as well as the large difference in fibrillation micromechanics between the smooth and rough interface, was attributed to an inhomogeneous interface load, caused by locally interlocking areas in the valleys of the roughness and cavitation at the peaks of the roughness. Arguably, this fibrillation process spreads the energy dissipation over a larger (process) zone by forcing the interface crack to arrest and even kink or branch away from the interface and into the bulk materials.

Peel tests at a wide range of peel rates provided new insight in the delamination micromechanisms, such as the extent of crack branching into the TPU fibrils. From a detailed microscale analysis, it was observed that the macroscopically observed increase of the work of separation (WOS) with increasing peel rate is due to an increase in flow stress of the TPU material within the process zone, probably accompanied by more effective mechanical interlocking at high peel rates. Finally, it was found that the major contribution of the work of separation is the consequence of the fibrillation process, i.e. the formation, stretching, and rupture of the fibrils, where part of the energy is dissipated viscously, and by dynamically dissipating the elastically stored energy in the fibrils, or in the near-fibril bulk material, released upon fibril rupture. This last dissipation mechanism is also suggested from numerical multi-scale investigations of PDMS-Copper interfaces by Vossen et al. [23].

In the fibrillation mechanism, a delicate balance exists between the fibril debonding at the interface and fibril rupture. If the (microscale) fibril-copper adhesion is insufficient, the fibrils will debond before building up strain energy and reaching their full dissipative capacity. Therefore, the key to optimize the fracture toughness is to maximize the allowable tractions of the fibrils, for which a strongly interlocking structure is required at the base of the fibrils. One way to achieve this, is by employing similar high roughness interfaces as the ones investigated here. This is indeed being applied in large-area stretchable electronics (demonstrators), because these applications allow for relatively large interconnect sizes. It is interesting to see if an artificial roughness, designed to initiate cavitation and interlocking, can initiation fibrillation and provide similar enhancements in fracture toughness.

Acknowledgment

T. Löher of the University of Berlin is gratefully acknowledged for his support and input in this research, and for providing sample materials. Additionally, the following students are acknowledged for their contributions; O. Sedaghat, A.P. Ruybalid, K. Hu, T. v. Lochem, U. Hoeberichts, and J.L.T.P. Basten. Finally, M.P.F.H.L. van Maris is acknowledged for his general technical support on the experiments. This work has been supported by the Dutch Technology Foundation (STW) and the Dutch Organization for Scientific Research (NWO).

References

[1] Creton, C., Hooker, J. C., Shull, K. R., 2001. Bulk and interfacial contributions to the debonding mechanisms of soft adhesives: Extension to large strains. Langmuir 17 (16), 4948–4954.

[2] Creton, C., Kramer, E. J., Hui, C. Y., Brown, H. R., 1992. Failure mechanisms of polymer interfaces reinforced with block copolymers. Macromolecules, 3075–3088.

[3] Crosby, A. J., Shull, K. R., Lakrout, H., Creton, C., 2000. Deformation and failure modes of adhesively bonded elastic layers. Journal of Applied Physics 88 (5), 2956–2966.

[4] Eyring, H., 1936. Viscosity, Plasticity, and Diffusion as Examples of Absolute Reaction Rates. The Journal of Chemical Physics 4 (4), 283.

[5] Geißler, G., Kaliske, M., 2010. Time-dependent cohesive zone modelling for discrete fracture simulation. Engineering Fracture Mechanics 77 (1), 153–169.

[6] Hoefnagels, J. P. M., Neggers, J., Timmermans, P. H. M., van der Sluis, O., Geers, M. G. D., 2010. Copper-rubber interface delamination in stretchable electronics. Scripta Materialia 63, 875–878.

[7] Hsu, Y.-Y., Gonzalez, M., Bossuyt, F., Axisa, F., Vanfleteren, J., de Wolf, I., 2009. In situ observations on deformation behavior and stretching-induced failure of fine pitch stretchable interconnect. Journal of Materials research, 3573–3582.

[8] Hsu, Y.-Y., Gonzalez, M., Bossuyt, F., Axisa, F., Vanfleteren, J., de Wolf, I., 2010. The effect of pitch on deformation behavior and the stretching-induced failure of a polymer-encapsulated stretchable circuit. Journal of Micromechanics and Microengineering 20 (7), 1–11.
[9] Hsu, Y.-Y., Gonzalez, M., Bossuyt, F., Axisa, F., Vanfleteren, J., Vandevelde, B., de Wolf, I., 2010. Design and analysis of a novel fine pitch and highly stretchable interconnect. Microelectronics International 27 (1), 33–38.
[10] Hutchinson, J. W., Suo, Z., 1992. Mixed mode cracking in layered materials. Advances in applied mechanics 29, 63–191.
[11] Kendall, K., 1975. Thin-film peeling-the elastic term. Journal of Physics D: Applied Physics 8 (13), 1449–1452.
[12] Kim, J. K., Sham, M. L., 2000. Impact and delamination failure of woven-fabric composites. Composites Science and Technology 60, 745–761.
[13] Kim, K.-S., Aravas, N., 1988. Elastoplastic analysis of the peel test. International Journal of Solids and Structures 24 (4), 417–435.
[14] Li, T., Huang, Z. Y., Xi, Z. C., Lacour, S. P., Wagner, S., Suo, Z., 2005. Delocalizing strain in a thin metal film on a polymer substrate. Mechanics of Materials 37 (2-3), 261–273.
[15] Liechti, K. M., Wu, J. D., 2001. Mixed-mode, time-dependent rubber/metal debonding. Journal of the Mechanics and Physics of Solids 49, 1039–1072.
[16] Loeher, T., Manessis, D., Heinrich, R., Vanfleteren, J., DeBaets, J., Ostmann, A., Reichl, H., 2006. Stretchable electronic systems. Electronics Packaging Technology Conference, 271–276.
[17] Tvergaard, V., Hutchinson, J. W., 1993. The influence of plasticity on mixed mode interface toughness. Journal of the Mechanics and Physics of Solids 41 (6), 1119–1135.
[18] van den Bosch, M. J., Schreurs, P. J. G., Geers, M. G. D., van Maris, M. P. F. H. L., 2008. Interfacial characterization of pre-strained polymer coated steel by a numerical-experimental approach. Mechanics of Materials 40 (4-5), 302–317.
[19] van der Sluis, O., Hsu, Y.-Y., Timmermans, P. H. M., Gonzalez, M., Hoefnagels, J. P. M., 2011. Stretching-induced interconnect delamination in stretchable electronic circuits. Journal of Physics D: Applied Physics 44, 034008.
[20] van der Sluis, O., Remmers, J. J. C., Thurlings, M. A. C., Welling, B. J., Noijen, S. P. M., 2014. The competition between adhesive and cohesive fracture at a micro-patterned polymer-metal interface. Key Engineering Materials 577-578, 225–228.
[21] van der Sluis, O., Yuan, C. A., van Driel, W. D., Zhang, G. Q., 2008. Advances in Delamination Modeling. In: Nanopackaging. Ch. 4, pp. 61–91.
[22] Vella, D., Bico, J., Boudaoud, A., Roman, B., Reis, P. M., 2009. The macroscopic delamination of thin films from elastic substrates. Proceedings of the National Academy of Sciences of the United States of America 106 (27), 10901–10906.
[23] Vossen, B. G., Schreurs, P. J. G., van der Sluis, O., Geers, M. G. D., 2014. Multi-scale modelling of delamination through fibrillation. Journal of the Mechanics and Physics of Solids 66, 117–132.
[24] Wagner, S., Lacour, S. P., Jones, J., Hsu, P.-h. I., Sturm, J. C., Li, T., Suo, Z., 2004. Electronic skin: architecture and components. Physica E: Low-dimensional Systems and Nanostructures 25 (2-3), 326–334.
[25] Wei, Y., Hutchinson, J. W., 2007. Peel Test and Interfacial Toughness. In: Comprehensive Structural Integrity. Elsevier, Oxford, Ch. 8.05, pp. 18–217.
[26] Xu, W., Yang, J. S., Lu, T. J., 2011. Ductility of thin copper films on rough polymer substrates. Materials & Design 32 (1), 154–161.
[27] Yao, Q., Qu, J., 2002. Interfacial Versus Cohesive Failure on Polymer-Metal Interfaces in Electronic Packaging-Effects of Interface Roughness. Journal of Electronic Packaging 124, 127–134.